energies

MDPI

Article

A System-Level Modeling of PEMFC Considering Degradation Aspect towards a Diagnosis Process

Antoine Bäumler [1], Jianwen Meng [1], Abdelmoudjib Benterki [1], Toufik Azib [1,*] and Moussa Boukhnifer [2]

[1] ESTACA, ESTACA'Lab—Paris-Saclay, F-78180 Montigny-le-Bretonneux, France; antoine.baumler@estaca.fr (A.B.); jianwen.meng@estaca.fr (J.M.); abdelmoudjib.benterki@estaca.fr (A.B.)
[2] Laboratoire de Conception, Optimisation et Modélisation des Systèmes, Université de Lorraine, F-57000 Metz, France; moussa.boukhnifer@univ-lorraine.fr
* Correspondence: toufik.azib@estaca.fr; Tel.: +33-1-76-52-11-03

Abstract: This paper proposes a modular modeling towards a health system integration of fuel cells by considering not only the dynamics of the gases but also fault models that affect the PEMFC performances. The main goal is to simulate the faulty state in order to overcome data scarcity, since running a fuel cell to generate a database under faulty conditions is a costly process in time and resources. The degradation processes detailed in this paper allow to introduce a classification of faults that can occur, giving a better understanding of the performance losses necessary to simulate them. The faults that are detailed and modeled are the flooding, drying and aging processes. This modeling is based on a system approach, so it runs faster than real-time degradation tests, allowing the training and validation of online supervisors, such as the energy management strategy (EMS) method or diagnosis. The faults are reproduced according to the study requirements to be a very effective support tool to help design engineers to include faulty conditions in early design stages toward a diagnosis process and health-conscious energy management strategies.

Keywords: PEMFC modeling; PEMFC faults; water management; FC diagnosics

Citation: Bäumler, A.; Meng, J.; Benterki, A.; Azib, T.; Boukhnifer, M. A System-Level Modeling of PEMFC Considering Degradation Aspect towards a Diagnosis Process. *Energies* **2023**, *16*, 5310. https://doi.org/10.3390/en16145310

Academic Editor: Ahmad Baroutaji

Received: 16 June 2023
Revised: 5 July 2023
Accepted: 7 July 2023
Published: 11 July 2023

1. Introduction

The interest for sustainable energy sources for transportation applications is growing, since the combustion engine has led to a lot of environmental issues, such as air pollution, greenhouse gases emissions, noise and fossil fuel dependency. Currently, the most promising solution to alleviate these problems is electrification [1]. Although, this solution can reduce the environmental and social impacts of conventional vehicles, it comes with some drawbacks, such as driving range, security, dynamic performance, refueling, acquisition and operating cost and durability. The most competitive concept is the Battery Electric Vehicle (BEV) using lithium technology, with its satisfactory power and energy density. However, it presents some issues like vehicle range, long charging time and massive use of rare metals. One other promising concept is the fuel cell hybrid electric vehicle (FCHEV) powered by hydrogen, particularly using Proton Exchange Membrane Fuel Cell (PEMFC) technology [2].

Indeed, the operating temperature range of PEMFCs is between 50 and 80 °C [3], which is suitable for vehicular application, which requires a fast start-up. It also has a high energy density, where FCHEV can reach ranges and refueling times that compete with internal combustion engine vehicles. However, PEMFCs still have many issues and challenges, such as durability and reliability, acquisition cost, hydrogen production and efficient reversible energy storage. According to the European Union fuel cell and Hydrogen joint undertaking [4], the durability of FCs for light-duty vehicles was 4000 h in 2017, and the target is 6000 h in 2024. This can be achieved by improving the design and system integration. This last level implies introducing the hybridization concept by using a reversible energy sources to improve the durability (dynamics, start and stop, etc.)

and energy efficiency (reversibility, downsizing, reconfiguration, etc.). These challenges are related to FC use, which requires a reliable fault detection method and an efficient EMS. Thus, developing a reliable fault detection method is quite a challenge due to data scarcity and the high cost of operating FCs for several hours. Hence, one way to drastically reduce the cost is to develop a relevant system for FC modeling by considering different aspects: the dynamics, the faults and the aging of the FC.

The authors in [5,6] present a three-dimensional model of a PEMFC, which describes the effect of CO and CO_2 on the membrane electrode assembly (MEA) and the distribution of the water content on the membrane. In [7], the V-ribbed channel design is compared with the serpentine channel, using the CFD modeling of a PEMFC. A CFD model of the water flow in the GDL is proposed in [8], which gives an overview of where and how the water blocks the flow of gases in the channels. The modeling method based on CFD is a strong tool to precisely describe the PEMFC's dynamical behavior, considering the flow of gases in the channels. However, this method is computationally expensive and thus not suited for long-term use. Zhong et al. [9] proposed a black box model based on SVM to predict the voltage given the input parameter, such as current temperatures, pressures and membrane water content. In [10], a machine-learning-based model is also presented using a neural network. The model successfully predicts the output voltage and the resistance and membrane water content. Machine learning is a powerful tool to model PEMFCs; however, the precise behavior of the system is not known due to "black box" modeling. It also does not allow to precisely describe the faults inside PEMFCs, where the behavior is less predictable and very different depending on the situation. For this purpose, this paper proposes a system-based model of PEMFCs, with the dynamics of the fluids, simulating water management issues, such as drying and flooding, and taking into account the aging process. The main contribution of this study related to the existing published works is the system modeling, which simultaneously takes into account the dynamics, water management and aging process of PEMFCs. It is a very effective support tool toward diagnosis processes and health-conscious energy management strategies. Indeed, many research studies have been devoted to this topic in the literature [11–14]. Most of them provide a solution only for specific aspects, using complex computational techniques. For example, the authors in [11,12] modeled the flooding behavior in the gas diffusion layer (GDL) with the computational fluid dynamics method. This approach is well-suited to optimize the design of FCs and water management strategies, but it cannot be integrated into a system-based model due to computational cost. Others, such as refs. [13,14], proposed aging models that only depend on time, but the FC's demanded load greatly affects aging, which needs to be considered. For this, the aging of the proposed model depends on the FC demanded load, which better describes the aging process.

This paper is organized as follows: Section 2 introduces the faults of the fuel cell related to water management, including membrane drying and gas diffusion layer (GDL) flooding, poisoning, starvation and short circuits. Then, Section 3 presents each type of PEMFC modeling: a simple static model, a dynamical model and, ultimately, the main contribution, the faulty model, with the faults and aging process proposed by this paper. Finally, the simulation results are presented, and the validity of the model is discussed. Figure 1 gives an overview of the system modeling proposed in our paper, with the selected faults and the important parameters useful for diagnosis as input and output.

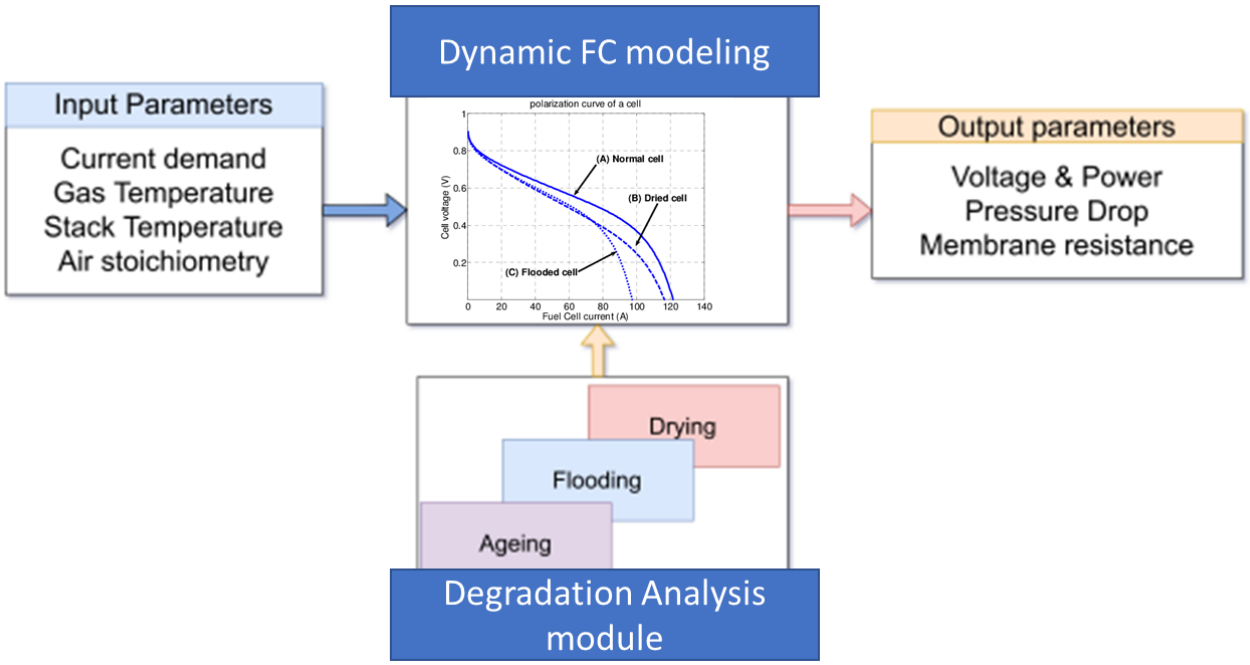

Figure 1. Proposed model summary with the adjustable parameters impacting the FC faults as input and the interesting parameters for diagnosis at the output.

2. PEMFC Faults and Degradation

An FC stack includes several cells; each cell is composed of three main components, the GDL, where all the reactants are spread, the electrodes (anode and cathode), allowing the reaction to happen and collecting the electrons, and the membrane, which is permeable to electrons while allowing the protons to pass through. There are many factors that influence the degradation of FCs: high load variations, low and high operating conditions and start/stop cycles [15,16]. The faults are also involved in the degradation process of FCs, having an irreversible and reversible impact on performance losses. We can cite the water management, characterized by the flooding and drying of the membrane, the fuel starvation that can corrode the electrodes and short circuits and poisoning. According to [17], the water management fault represents 52% of the irreversible performance degradation in general, based on the data extracted from different papers. This result will highly depend on how the fuel cell is operated and the design of the GDL. The poisoning effect, meanwhile, refers to the presence of impurities in the reactant, it can be at the anode side, with the presence of CO (carbon monoxide) coming from the methane reformatting or at the cathode, with the presence of pollutants such as NO_x and SO_2 coming from the exhaust gas of internal combustion engine cars [18]. The short circuit refers to the high current that causes local high temperature on the membrane, which can lead to the development of pinholes [19], causing total failure of the cell. In [20], a summary of the catalyst degradation in the form of a fault tree is proposed; in [21], a similar type of classification is suggested, summarizing the water management (drying and flooding) issues. These classifications give an overview of the operating condition of the FC's components and operating parameters that permanently degrade the components; thus, the signature of the faults are not detailed here, which are crucial to understand and diagnose performance losses. Indeed, in order to make a more relevant classification of FC faults and to better understand the main performance degradation mechanism and their signature that allows to detect them, we propose the taxonomy shown in Figure 2.

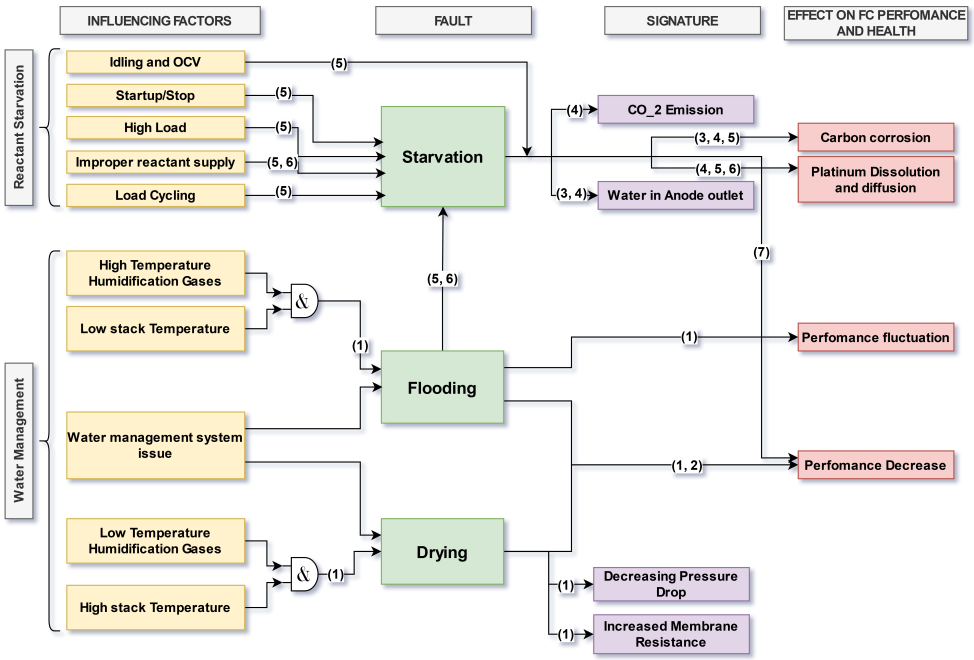

Figure 2. Fault summary occurring in the FC, with its effect on performance and signature: (1) Barbir et al., 2004 [22], (2) Hui Li et al., 2007 [23], (3) Baumgartner et al., 2008 [24], (4) Xia et al., 2023 [25], (5) Yousfi-Steiner et al., 2009 [20], (6) Taniguchi et al., 2008 [26] and (7) Manokaran et al., 2015 [27].

The poisoning and short-circuit effects are not considered in this study. Indeed, the poisoning effect depends on the external parameters, such as the hydrogen production method and air pollution [28]. The short circuit happens quickly, so it cannot be detected in time [29]. Starvation is partly modeled here with aging, and it is also linked to the model with the flooding fault. The rest of this section gives an overview of the starvation issue and water management

2.1. Reactant Starvation

The fuel starvation fault refers to an undersupply of reactant in the cell. It can be a local phenomenon if the reactant supply is uneven or global, where the whole reactant supply system is faulty [20]. The starvation can be either at the anode or cathode side, respectively, referring to the undersupply of fuel (hydrogen) or oxidant.

2.1.1. Fuel Starvation

Fuel starvation happens when there is an issue in the supply of hydrogen to the MEA, which leads to an accelerated degradation of the fuel cell. This lack of supply is due to many reasons [20]: (i) an undersupply in H_2 caused by a leak in the GDL, (ii) variation in the load demand (the dynamic of the supply system might not follow if the load demand variation is too fast [30]), (iii) the start-up of the FC, which is even more severe when the shutdown time is longer because of the presence of air inside the anode which blocks the passage of hydrogen [24,31], (iv) an unprotected shutdown, where residues of reactant are present in the GDL and the FC is under the OCV (Open-Circuit Voltage) condition, which resembles the condition for electrode corrosion [32] and (v) high load demand, thus lowering the partial pressure of the reactant.

2.1.2. Oxidant Starvation

More localized starvation occurs when the membrane is flooded; as presented before, the water molecules block the gas flow in the GDL or on the reaction sites of the electrodes, thus creating areas where the reaction cannot happen [22].

At high load demand, where the fuel cell performance is located in the concentration loss region, starvation can also occur due to the high consumption of the reactant reducing the partial pressure of the oxidant.

2.1.3. Effect on Performance and Aging

At the cathode, where the irreversible degradation is the most pronounced, the catalyst and the carbon support of the electrode can oxidize and corrode in starvation [33,34].

$$C + 2H_2O \rightarrow CO_2 + 4H^+ + 4e^- \quad (1)$$

$$Pt + xO_2 \rightarrow PtO_{2x} \quad (2)$$

Equations (1) and (2) show the processes of carbon support degradation and platinum oxidizing. Durst et al. [35] studied the effect of start/stop cycling on the performance of the fuel cell, which leads to starvation. They showed a degradation in the polarization curve and that the degradation was more significant at the inlet of the cell. Manokaran et al. [27] observed the same effect. They ran a fuel cell in an oxidant and hydrogen starvation condition and measured the current density and potential at different spots on the reactant channel flow to determine the effect on performance. The experiments were run at constant voltage and at constant current. When the current is set, the current density is much higher at the inlet than at the outlet, leading to a local starvation and an accelerated degradation.

2.2. Water Management

For a proper operation of the FC, the amount of water inside the GDL and membrane must be monitored. The FC can produce a large quantity of liquid water, degrading the performance. On the contrary, if the water becomes scarce in the membrane, then the drying phenomenon occurs, also decreasing the performance [36].

2.2.1. Flooding

The flooding of the membrane is characterized by increased water content in the Nafion membrane and the presence of liquid water in the GDL. This behavior is influenced by the temperature of the stack and the input air, the inlet relative humidity of reactants, their stoichiometry and the load profile of the FC. These parameters are influenced by the water management strategy and the profile of the demanded load; if the load rises quickly, the water removal system might not properly follow.

There are several levels of flooding depending on the type of flow inside the GDL. As there are multiple phases inside the channels (liquid and gaseous), the flow of reactants can be slower. The most common flows are known as single-phase flow (gaseous only), bubbly flow, film flow and slug flow [37]. The different flow types are shown in Figure 3. When all the water is vaporized, thus at gaseous state, the flow is at single-phase flow. If more water is produced by the FC reaction, so that it is at saturation pressure, bubbles appear which are tinier than the channel section and stick to the surface of the GDL due to surface tension [38,39]. When even more water is produced, the bubbles merge and form a film of water, flowing along the channel's walls, and finally, with an even higher water production rate, the liquid flow of water agglomerates as a slug, which obstructs the GDL.

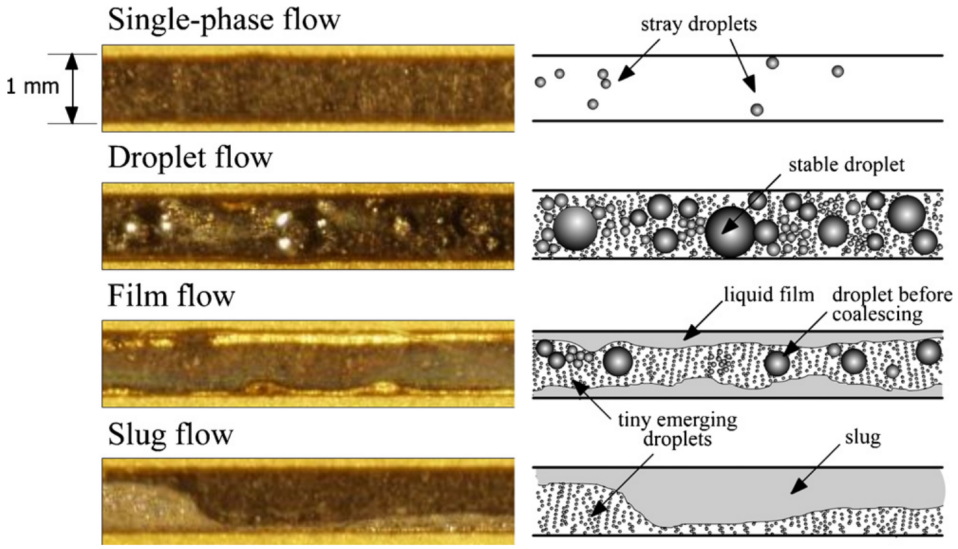

Figure 3. Magnified view of flow patterns in the channels [40].

The most used parameter for detecting water management issues, besides voltage evolution, is the pressure drop [21,22]. The signature and effect on performance is different according to the type of flow. According to the experiment by Grimm et al. [41], when no water formation or bubbles are observed, the pressure drop is rather constant. However, when a film of water is formed on the sidewall of the GDL, the pressure drop variations have a relatively high frequency with low amplitude. Finally, when slugs of water are present, the pressure drop variation is at low frequency and high amplitude due to water blocking the flow of gases and being flushed when the pressure reaches its peak. The flooding has the effect of blocking the passage of reactants along the GDL and across the membrane, thus reducing the performance, which can be observed by measuring the voltage drop. It can also be seen as a brief loss of active surface of the membrane electrode assembly (MEA), causing local starvation, which permanently degrades the FC. The pressure drop signature of each flow is summarized in Figure 4.

2.2.2. Drying

On the other hand, when the water supply is too low, the membrane tends to dry out, which increases the resistance to the passage of protons, thus reducing the voltage for a given current density. It can also lead to a severe and irreversible degradation, such as pinhole and delamination in a short amount of time [42]. To have better conductivity, the Nafion membrane needs to be humidified properly; to achieve this, water needs to be brought at the input of the fuel cell by means of air humidity.

The water content λ is a way to model the drying of the membrane, which is the number of water molecules per $SO_3^- H^+$ sites of the membrane. A correlation between the relative humidity, the water content and finally the ohmic losses of the membrane has been established by Springer et al. [43]. The drying out of the membrane occurs if the relative humidity at the entry is too low, combined with a high cell temperature compared with the input air, causing the evaporation of water in the membrane [22]. This is one of the reasons why a humidifier and a proper cooling system is crucial for an optimal FC operation.

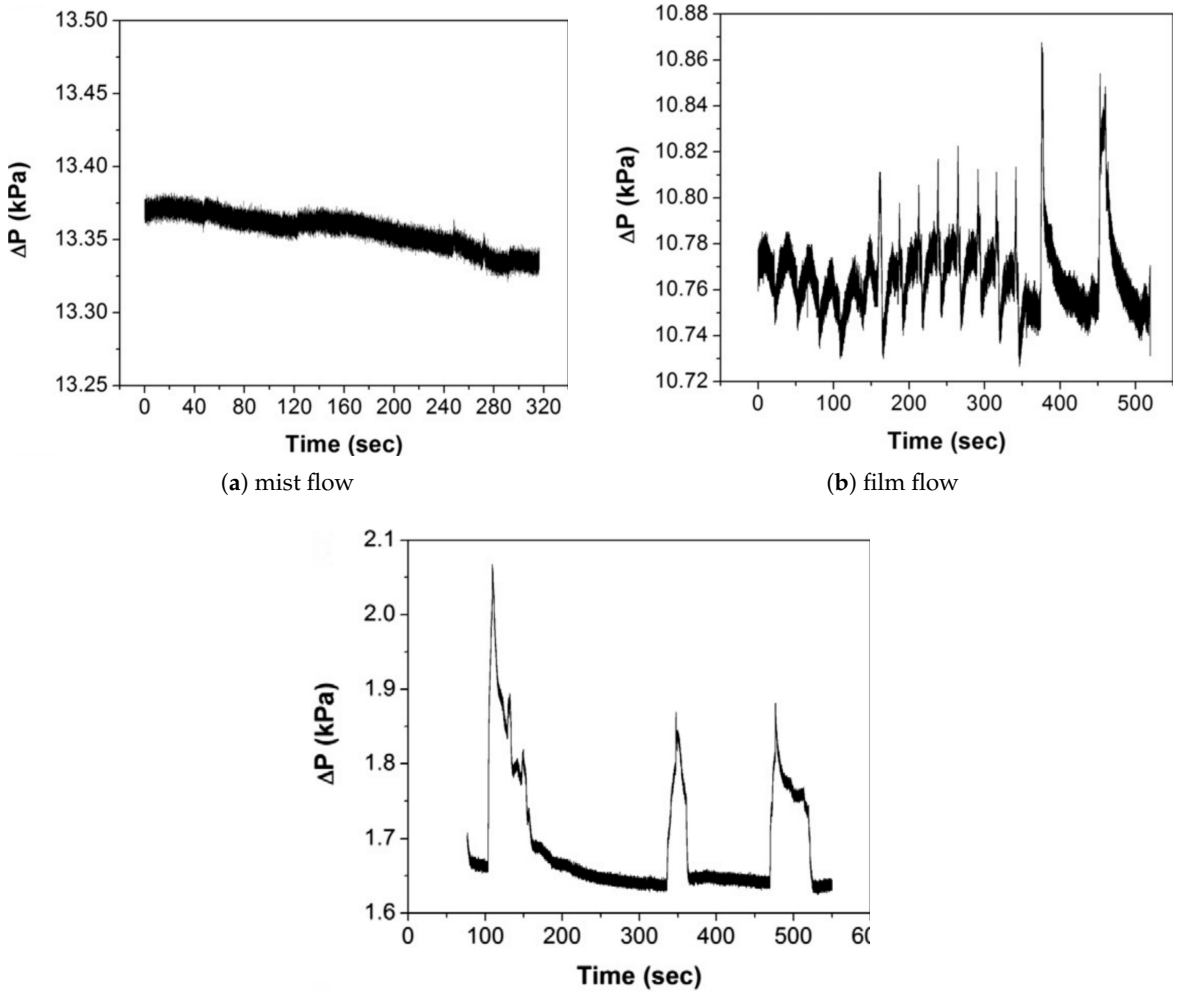

(**a**) mist flow (**b**) film flow

(**c**) slug flow

Figure 4. Pressure drop signature for each flow [41].

3. PEMFC Model and Fault Modeling

3.1. PEMFC Static and Dynamical Models

The behavior of a fuel cell can be characterized by its polarization curve, where voltage is plotted in function of the output current. The curve is built with the OCV and three losses: the activation losses, the ohmic losses and the concentration losses that depend on the current required from the PEMFC. Figure 5 shows the main loss zones depending on the current density.

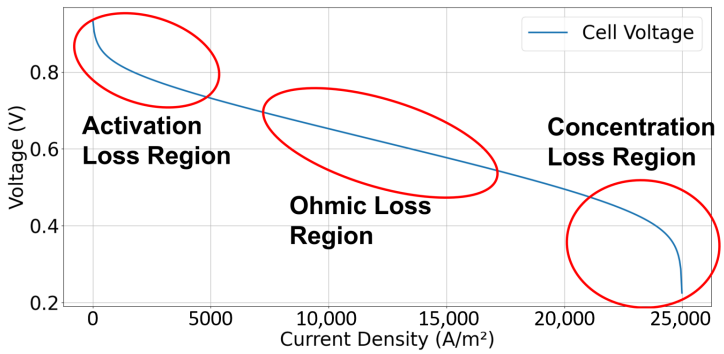

Figure 5. FC polarization curve with dominant loss region.

The OCV, or reversible voltage, is a function of partials pressures of the gases and is often represented with the Nernst equation:

$$V_0 = -\frac{\Delta G_f^0(T)}{2F} + \frac{R \cdot T}{2F} \ln\left(\frac{p_{H_2} \cdot p_{O_2}^{1/2}}{p_{H_2O}}\right) \tag{3}$$

where $\Delta G_f^0(T)$ is the free energy change for the FC reaction, p_{H_2}, p_{O_2}, $p_{H_2O}(Pa)$, respectively, the partial pressure of hydrogen in the anode and oxygen and water at the cathode. For a static model, the OCV is constant, as the dynamics of the reactants, i.e., the partial pressures, are considered as constant.

The activation losses represent the energy needed for the reaction to take place; it has a logarithmic behavior, where it increases quickly at very low current and is rather constant with higher loads. It is generally represented with the equation as follows:

$$V_{activation} = A \cdot \ln\left(\frac{i}{i_0}\right) \tag{4}$$

where $A(V)$ is an empirical parameter depending on the operated fuel cell, i_0 ($\mathrm{A} \cdot \mathrm{m}^{-2}$) is the FC minimum current and i ($\mathrm{A} \cdot \mathrm{m}^{-2}$) is the cell current density.

The ohmic losses are the energy dissipated by heat due to the resistance of the membrane and electrodes, this irreversibility increases linearly with the current:

$$V_{ohm,static} = r \cdot i \tag{5}$$

where r ($\Omega \cdot \mathrm{m}^{-2}$) is the membrane and electrode resistance.

Consequently, the concentration losses describe the loss of reactant availability in the exchange surface. The reactant supply is insufficient for the reaction to happen properly, thus reducing the voltage. This last part can be represented with an exponential law or a negative logarithmic, where the voltage penalty rises quickly as it approaches the current density limit.

$$V_{concentration} = -B \cdot \ln\left(1 - \frac{i}{i_L}\right) \tag{6}$$

where i_L ($\mathrm{A} \cdot \mathrm{m}^{-2}$) is the current density limit and B is an empirical parameter that depends on the fuel cell and its operating mode. The final voltage of the cell is then given by

$$V_{cell} = V_0 - V_{activation} - V_{ohm} - V_{concentration} \tag{7}$$

There are several ways to model PEMFCs, such as the static [44], electrical [45] and dynamical [46] models. The electrical model is based on the equivalent circuit of the electrical behavior of the fuel cell. The fuel cell is then modeled as an RC circuit [47], but Belhaj et al. [45] found that an RL circuit is more representative of PEMFC behavior. The issue with this type of modeling is that it models the electrical part, but a fuel cell is an electrochemical device, where the chemical part with gas flows has to be taken into account. The static model just models the three losses presented earlier with a constant OCV, and the only input to compute the voltage is the current. The dynamical model, on the other hand, takes other parameters into account, such as pressures, temperatures, gas flow rates and their dynamics. When the dynamics is included, the polarization curve shows a hysteresis, as pictured in Figure 6. The voltage is lower when the current is rising than when it is decreasing, which depicts this hysteresis effect. This is due to the inertia of the compressor and results in more or less abundance of reactant in the FC. The hysteresis effect modeling is detailed in [46]. The equations governing the pressure and gas flow variations are also detailed in their paper. The voltage variation comes from the OCV part, which is a function of the gas pressure, as described in Equation (3).

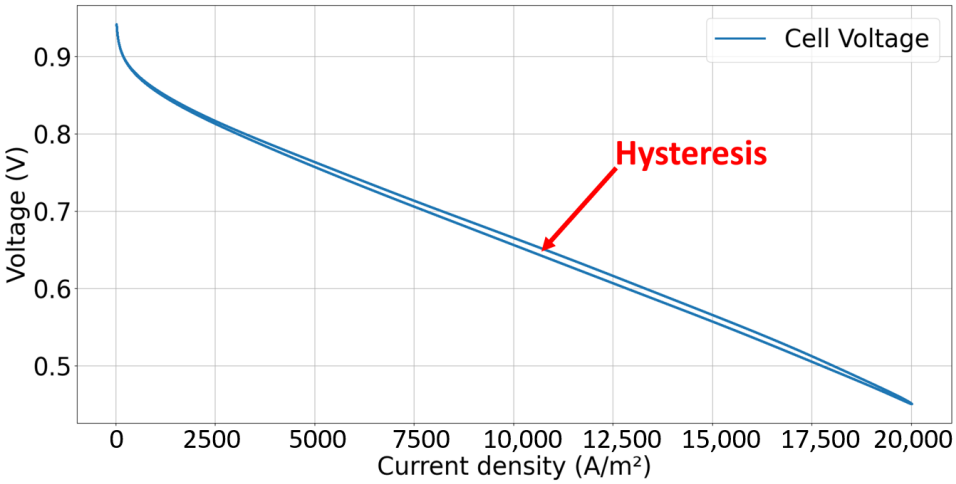

Figure 6. Polarization curve of the dynamical fuel cell model, with the hysteresis effect due to the compressor inertia.

To fit more with an actual state-of-the-art FC, the parameters used in this article are fitted with open databases. The dataset used comes from [48].

3.2. Proposed Model: Faults and Aging Model

3.2.1. Aging Model

As the fuel cell runs, the aging and improper use of the fuel cell reduce performance. The loss in performance can be modeled by an increased membrane and electrode resistance, which impact the generated power [22]. Jouin et al. [14] established a model with several parameters that vary through time to simulate the voltage loss to degradation because of its operation at a constant current of 0.7 A/cm^2. Bressel et al. [13] operated an FC under various cycles of current demand, with a relatively constant load for each cycle. The degradation modeling here is also time-dependent and modeled only on the resistive part of the FC model. Both models are time-dependent only and do not depend on the dynamics of the load, which has a great influence on the lifespan of PEMFCs, and it is all the more important for automotive applications [49].

Our study proposes to model the irreversible degradation of the FC with the data and coefficient used by Pei et al. [15] and integrates them into the ohmic losses, which results in

$$V_{ohm,ageing} = r_{ohm} \cdot i \cdot (1 + k_{deg} \cdot \alpha_{degradation}) \tag{8}$$

where k_{deg} is a degradation coefficient which must be fitted for each FC. The resistive term r_{ohm} is the resistance of the membrane and electrodes that is detailed in the next section.

$$\begin{aligned} \alpha_{degradation} = {} & k_{high.load}\delta t_{hl} + k_{low.load}\delta t_{ll} + k_{cycling}n_c \\ & + k_{start/stop}n_{s/s} + k_{operation}t_{op} \end{aligned}$$

where δt_{hl} and δt_{ll}, respectively, are the times spent at high load and low load, n_c is the number of high/low load cycling, $n_{s/s}$ is the number of fuel cell start and stop and t_{op} is the FC global operating time. Here, all the coefficients are taken from [15], with an additional coefficient, $k_{operation}$, which represents the natural degradation of the cell which, in this paper, is fitted on the database from the IEEE challenge [50], where the operating load of the fuel cell is rather constant.

3.2.2. Water Flux

As FCs have different types of water flows, it is crucial to model them to have a precise model that describes the drying and flooding faults. First, an FC produces water at a rate that is proportional to the current:

$$\dot{m}_{w,prod} = \frac{n_{cells} \cdot i_{fc} \cdot M_{H_2O}}{2F} \tag{9}$$

where n_{cells} is the number of cells in the FC stack, i_{fc} is the FC current and M_{H_2O} is the molar mass of water. Then, we have the water that comes with the air in the form of humidity:

$$\dot{m}_{w,in} = \frac{p_{sat} \cdot rh \cdot M_{H_2O}}{p_{air,in} \cdot M_{air}} \cdot \dot{m}_{ca,in} \tag{10}$$

where M_{air} is the molar mass of air, rh is the relative humidity of the input air, p_{sat} is the saturation pressure of water in air, $p_{air,in}$ is the pressure of the input air and $m_{ca,in}$ is the input flow of gases in the cathode. In addition, according to Karnik et al. [51], water can flow through the membrane due to the electro-osmotic drag from the cathode to the anode, which helps to hydrate the membrane and increase proton conductivity. The equations are detailed in this paper in Section 2.1.

3.2.3. Drying

As explained earlier, drying is due to the lack of water in the membrane, thus increasing the resistance of the fuel cell and increasing ohmic losses. The model used in this paper is the one proposed by Springer et al. [43], as follows:

$$V_{ohm,drying,ageing} = i \cdot \frac{t_m \cdot (1 + k_{deg} \cdot \alpha_{degradation})}{(0.00519\lambda - 0.00324) \cdot \exp(1268 * (\frac{1}{303} - \frac{1}{T}))} \tag{11}$$

where $\lambda_{(.)}$ is the water content, defined as the water content at the anode or the cathode:

$$\lambda_{(.)} = \begin{cases} 0.043 + 17.81 \cdot a_{w,(.)} - 39.84 \cdot a_{w,(.)}^2 & \\ +36.0 \cdot a_{w,(.)}^3 & 0 < a_{w,(.)} < 1 \\ 14 + 1.4(a_{w,(.)} - 1) & 1 < a_{w,(.)} < 3 \end{cases} \tag{12}$$

$a_{w,(.)}$ denotes the water activity (anode or cathode) at the cathode, which is given by

$$a_{w,ca} = \frac{\dot{m}_{w,in} + \dot{m}_{w,prod}}{\dot{m}_{w,sat}} \tag{13}$$

where

$$\dot{m}_{w,sat} = \frac{p_{sat,out} \cdot V_{ca} \cdot M_{H_2O}}{T \cdot R} \tag{14}$$

3.2.4. Flooding

In this paper, the flooding is discriminated into 3 levels: (i) no flooding, characterized by a single-phase or bubbly flow, (ii) partial flooding, with a film flow, and (iii) severe flooding, with a slug flow. The method used to discriminate each flow is based on the experimental results of Hussaini et al. [40], where the flow speed of each phase is put on a flow map and labels the type of flow according to the position on the flow map, as shown in Figure 7.

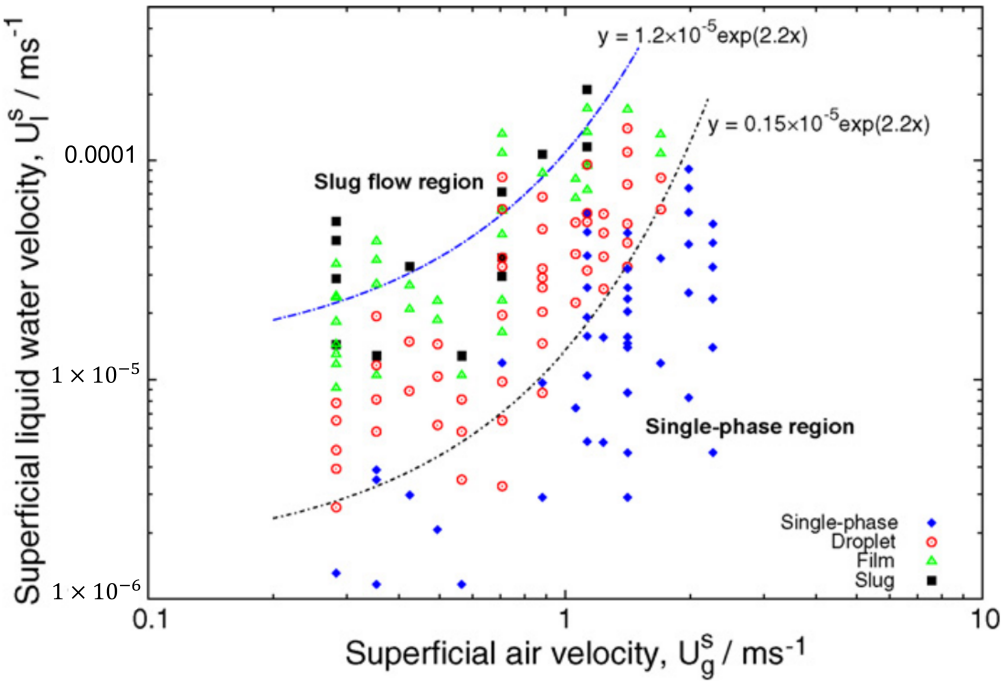

Figure 7. Cathode channel flow map [40] for flow type (single-phase, bubble and slug flow) classification.

The flow speed of the liquid and gaseous state is given by

$$U_{(.)} = \frac{W_{(.)}}{\rho \cdot S_{channel}} \tag{15}$$

where (.) stands for liquid or gaseous state. In the literature, the most used parameters to detect flooding are pressure drop and voltage. The performance loss is characterized in this model by reducing the active area of the fuel cell, which increases the current density, hence increasing the losses, resulting in a lower voltage for a given demanded current density. The behavior of the flooding fault can be qualified as random due to the lack of knowledge of the exact performance loss for the type of flow and quantity of liquid water. To model this at the beginning of the flooding fault, the initial degraded surface is a function of the water activity of the cathode, with a random noise to simulate this "random" behavior, modeled with the normal law $\mathcal{N}(\mu, \sigma)$. The initial loss of the active surface is given in the form of

$$S_{degraded} = S_{initial} \cdot (1 - \frac{a_{w,ca}}{\alpha_{severity}}) \cdot (1 - \mathcal{N}(0, \frac{a_{w,ca}}{\alpha_{severity}})) \tag{16}$$

Then, the loss is updated as

$$S_{degraded} = (S_{intial} - S_{degraded}) \cdot \alpha_{update\_rate} \tag{17}$$

where $S_{initial}$ is the healthy membrane area and $\alpha_{severity}$ is a coefficient to adapt according to the severity of the flooding, i.e., the type of flow. α_{update_rate} is the rate at which the membrane surface gets reduced. The behavior denoted in Figure 4 for the performance can be reproduced with this method. In order to determine the pressure drop of the two phases, the separate flow model proposed by Lockhart and Martinelli [52] is used. The pressure drop of each flow type can be simply calculated with the Hagen–Poiseuille equations as follows:

$$\Delta P_{(.)} = \frac{8\eta_{(.)}L}{\pi R^4} D_{v,(.)} \tag{18}$$

where $\eta(kg \cdot m^{-1} \cdot s^{-1})$ is the dynamical viscosity, $L(m)$ and $R(m)$ are the pipe length and diameter and $D_{v,(.)}(m^3 \cdot s^{-1})$ is the flow speed of the phase. The global pressure drop is then given by

$$\left(-\frac{dp}{dz}\right)_{TwoPhase} = \left(-\frac{dp}{dz}\right)_g + \left(-\frac{dp}{dz}\right)_l + C \cdot \left(\left(-\frac{dp}{dz}\right)_g \cdot \left(-\frac{dp}{dz}\right)_l\right) \tag{19}$$

The Chisholm parameter C is determined from the speed of the liquid phase U_l, and the water quality x is taken from the Grimm et al. paper [41]:

$$C = a \cdot \left(\frac{1-x}{x}\right)^b \tag{20}$$

where

$$a = \alpha_{1,(.)} \cdot U_l^{\alpha_{2,(.)}} \tag{21}$$

$$b = \beta_{1,(.)} \cdot U_l^{\beta_{2,(.)}} \tag{22}$$

where $\alpha_{(.)}$ and $\beta_{(.)}$ are some parameters to fit for the specific fuel cell.

4. Results

The FC is modeled, and the tests are performed using Python V3.10 with the basic libraries. The framework choice is motivated by the better control of the parameters. The FC considered here is a single cell with an active membrane area of 45 cm². The model is run on different current profile frequencies, which mostly influence the water management behavior. The requested current is a sinusoidal function with an amplitude covering the lowest to highest current density of the cell, which here is 2 A/cm^{-2} (90 A). This section shows the response of the dynamical model to the different load frequencies.

4.1. Influence of the Dynamics

In Figure 8, (a) is the load current density from 0 to 2 A/cm^{-2}, with a frequency of 0.01 Hz, and the degraded current density given by the FC model is shown, (b) is the corresponding voltage, (c) is the pressure drop and (d) is the membrane water content. (a) depicts spikes in the effective current density of the FC due to the flooding effect, which is reflected into (b) the voltage, where it drops at the current density spikes. The pressure drop fluctuations (c) are also more important in the flooding situations, as described in Section 2.2.1 and in the study by Grimm et al. [41]. The last plot (d) shows that water content drops at low current density due to reduced production of water, reducing the voltage in those conditions. It also happens when the pressure drop is low. The value of the membrane water content varies between 5 and 14, as given by Springer et al. [43].

Figure 9 is the flow map taken from [40], presented in Section 3.2.4, which allows discriminating the type of flow shown if Figure 8c.

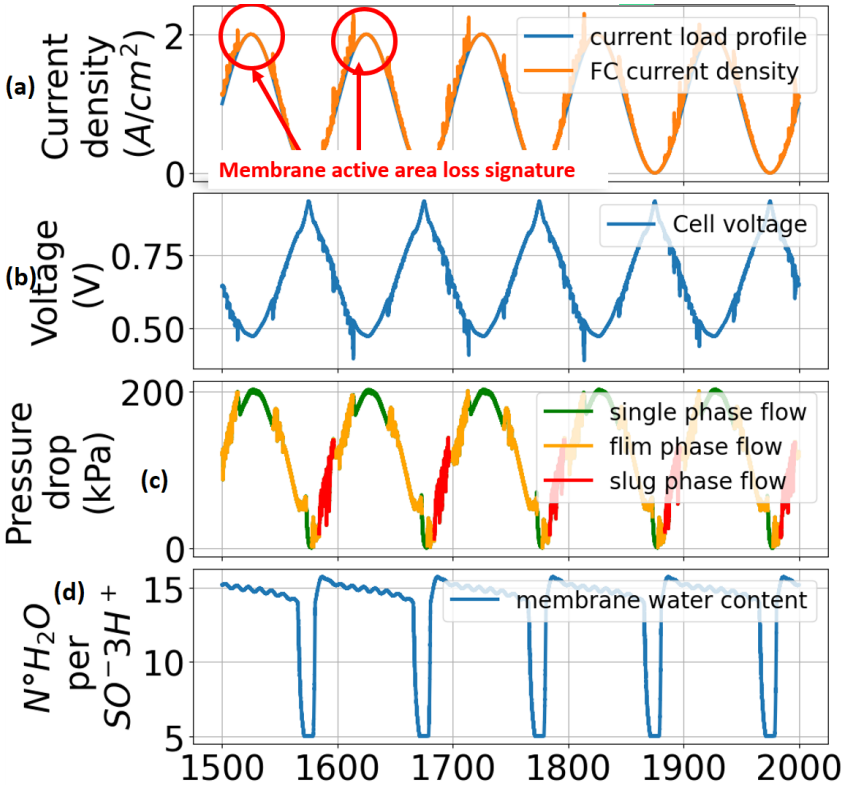

Figure 8. Cell behavior for the 0.01 Hz current density load: (**a**) demanded current vs FC current density, (**b**) voltage evolution of FC, (**c**) pressure drop with flow type discrimination and (**d**) membrane water content evolution.

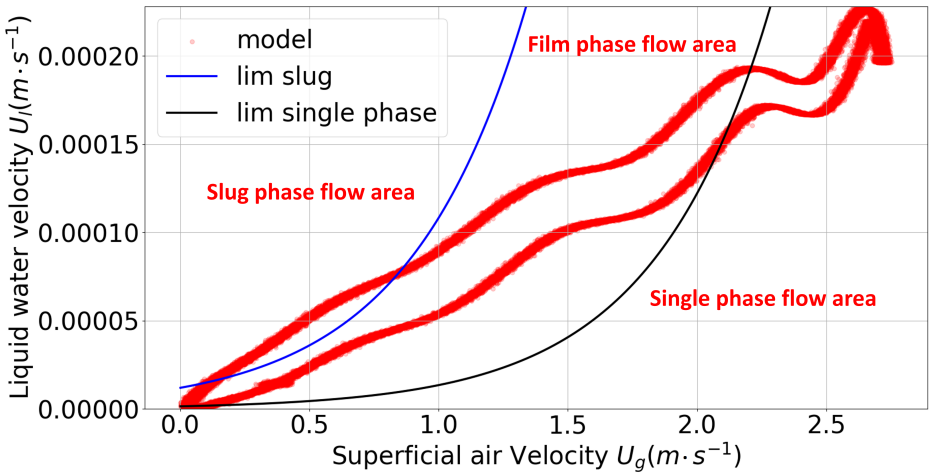

Figure 9. Flow map for a 0.01 Hz load demand for fault classification.

Figure 10 shows the same plots with a load frequency of 0.1 Hz. The flooding and drying effects are more pronounced is this load condition. When the membrane dries out, the pressure drop and the water content decreases, as described by Barbir et al. [22].

The comparison between a healthy and faulty FC is pictured in Figure 11, with their respective polarization curves. Two regions can be noticed: At low current densities, the voltage is significantly lower for the faulty FC, which is due to the drying effect of the membrane. At high current densities, the current density is higher due to the temporary loss of active surface due to flooding.

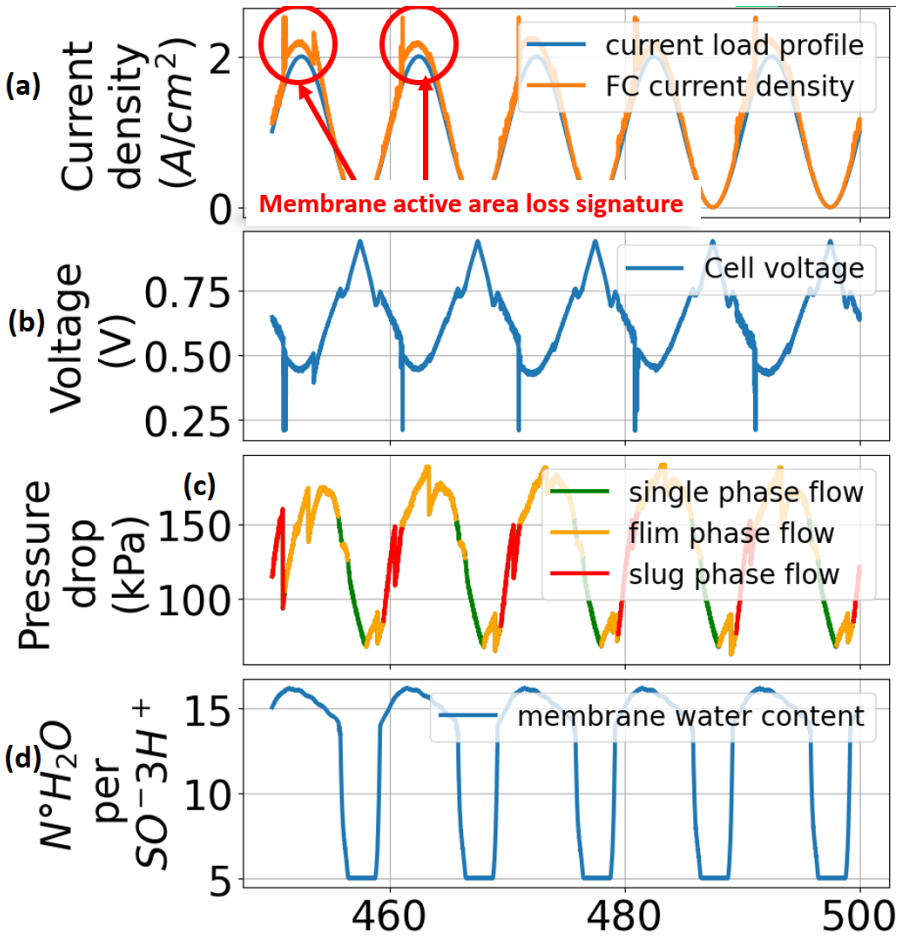

Figure 10. Cell behavior for a 0.1 Hz current density load. (**a**) load current density with membrane area loss signature, (**b**) voltage response, (**c**) pressure drop with type of flow, (**d**) membrane water content in drying conditions.

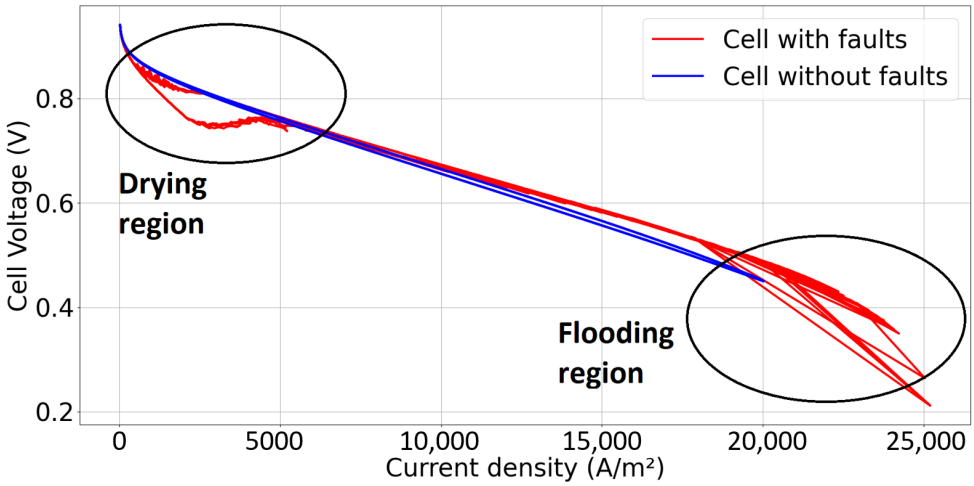

Figure 11. Polarization curve of the model with a load frequency of 0.1 Hz.

A 7% voltage loss due to drying is noticed here. This is crucial information to perform diagnosis processes and to guide the decision making of a health-conscious EMS.

Figure 12 shows the response of the model under a load frequency of 1 Hz. Here, the fault, flooding and drying are less important. In (d), the membrane water content varies between 13.5 and 15.5; because the membrane does not have time to dry out, there is still enough water from the last high load.

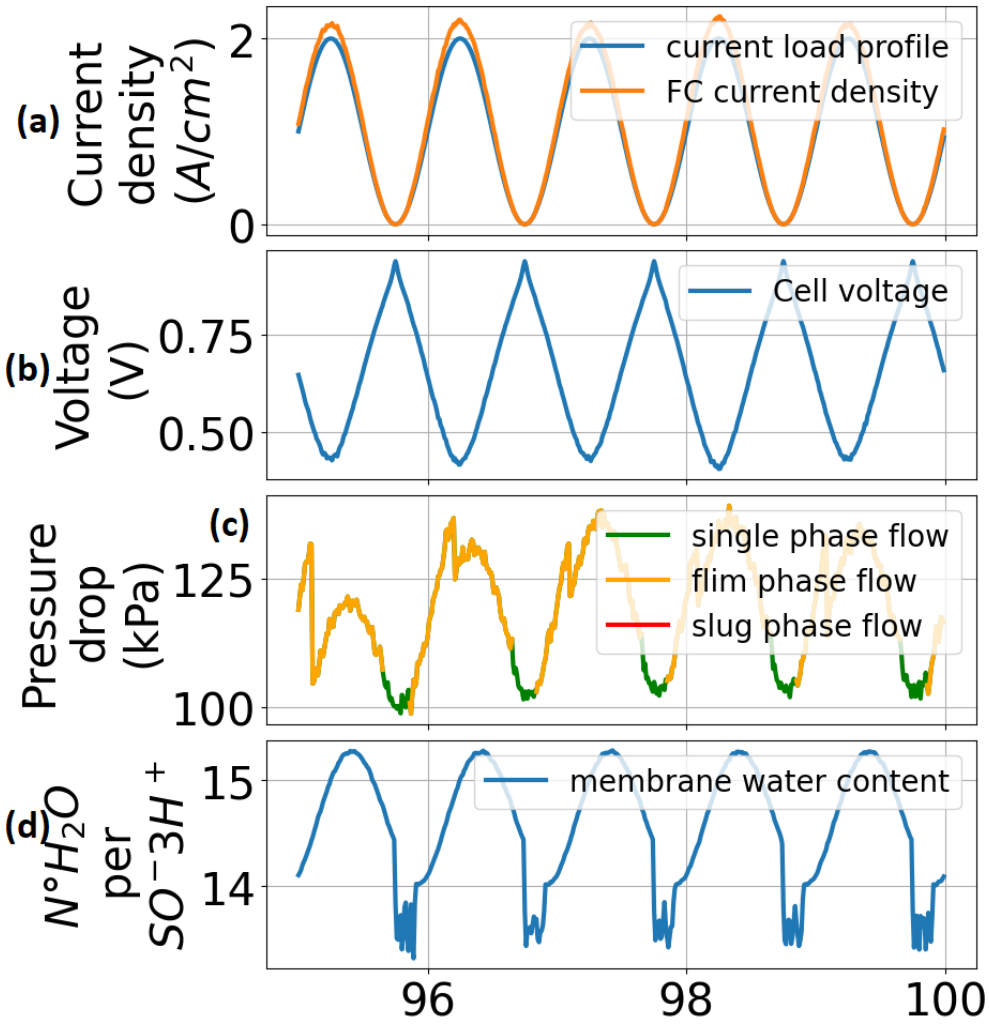

Figure 12. Cell output parameters: (**a**) load current density, (**b**) cell voltage, (**c**) pressure drop, (**d**) membrane water content evolution.

The behaviors presented here provide an insight into FC operating strategies, where, depending on the load profile, energy losses may be higher. This can be useful for selecting an EMS in the fuel cell load demand. In addition, the aging process must also be taken into account, which is presented in the next subsection.

4.2. Aging

As explained earlier, depending on how an FC is operated and its natural aging process, performance degrades. In Figure 13, the FC is run for 1750 h under a load cycle of 0.1 Hz, and a polarization curve is plotted every 250 h to give an overview of the progressive permanent degradation. The result shows that the polarization curve becomes lower in voltage over time for a given current density. The performance loss due to accelerated aging is modeled here by an increased resistance, which can be seen in the evolution of the polarization curves in the given plot.

The decrease in the maximum power of the FC is shown in Figure 14. With an end of life set at 20% of the maximum power loss, the simulated FC lasts around 1500 h, which matches with the rated lifespan of the Nexa1200 FC system [53].

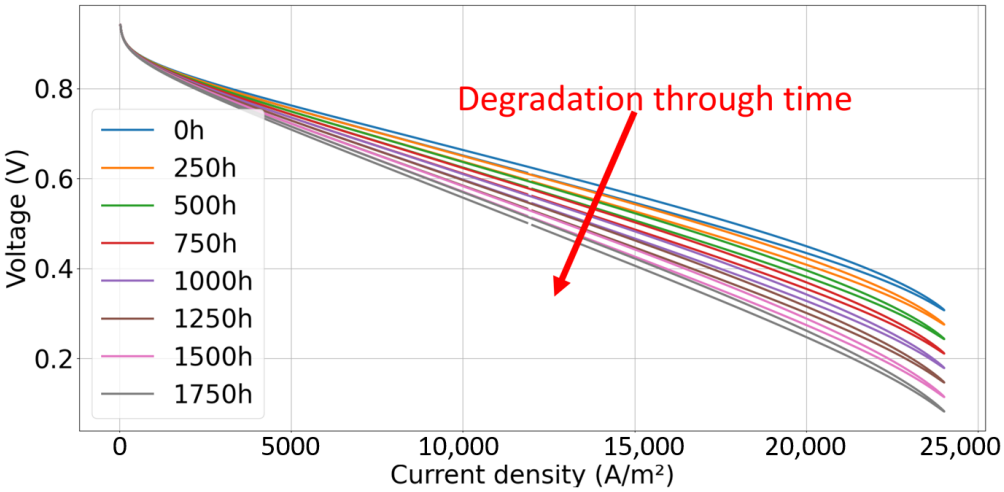

Figure 13. Polarization curve evolution in the aging process.

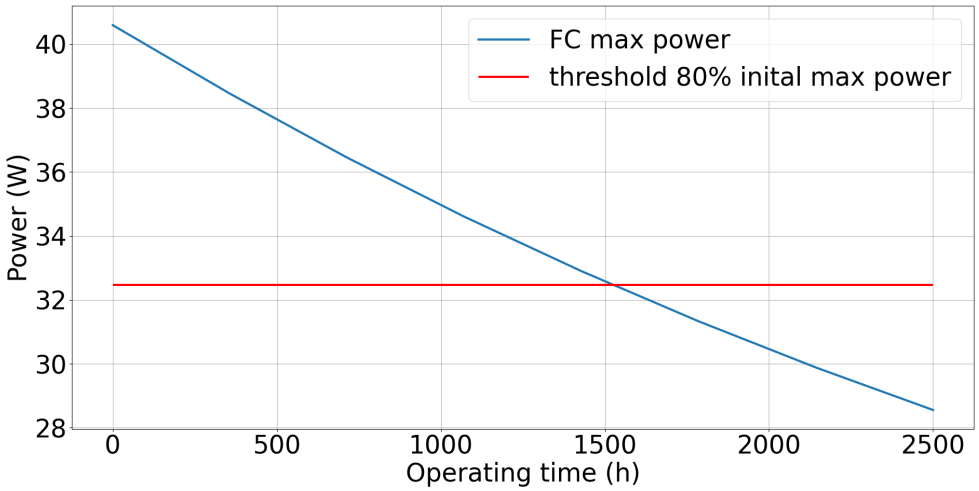

Figure 14. FC maximum power loss over time due to accelerated aging.

The rate at which the degradation occurs can be adjusted by changing the degradation weight (k_{deg}). With this approach, we point out that the approach is very simple, and the obtained results demonstrate its effectiveness and relevance. In addition, the degradation coefficient ($\alpha_{degradation}$) can be also extracted to give an overview of the evolution of the degradation, which can be useful for diagnosis and prognosis processes.

5. Conclusions

This paper presents a system-oriented dynamical PEMFC model, taking performance degradation into account. The hysteresis phenomenon is modeled through the internal dynamics of gases. Defects occur depending on the state of the water, whether it is liquid or gaseous. This offers a realistic modeling of the defects related to water management. On the other hand, the model requires data related to these defects in order to refine the coefficients and eventually correct the modeling equations in order to obtain a finer model on this type of degradation. However, this model is an introduction to FC fault modeling, taking into account water management and aging issues. It also allows a better understanding of the mechanisms reducing the performance of FCs.

This simulation is relevant for FC system applications. It can be used for diagnostic and prognostic purposes. Moreover, a health-conscious EMS requires a test environment allowing the validation of the energy management by taking into account the faults that

can occur within the fuel cell. It is a powerful tool to increase FC market penetration by using FCs in their best operating conditions.

Author Contributions: Conceptualization, A.B. (Antoine Bäumler), J.M., A.B. (Abdelmoudjib Benterki) and T.A.; methodology, A.B. (Antoine Bäumler), J.M., A.B. (Abdelmoudjib Benterki) and T.A.; software, A.B. (Antoine Bäumler); validation, A.B. (Antoine Bäumler), J.M., A.B. (Abdelmoudjib Benterki) and T.A.; writing—original draft preparation, A.B. (Antoine Bäumler), J.M., A.B. (Abdelmoudjib Benterki) and T.A.; writing—review and editing, A.B. (Antoine Bäumler), J.M., A.B. (Abdelmoudjib Benterki), M.B. and T.A.; supervision, M.B. and T.A. All authors have read and agreed to the published version of the manuscript.

Funding: This research received no external funding.

Data Availability Statement: No new data.

Conflicts of Interest: The authors declare no conflict of interest.

Abbreviations

The following abbreviations are used in this manuscript:

EMS	Energy Management Strategy
BEV	Battery Electric Vehicle (BEV)
FCHEV	Fuel Cell Hybrid Electric Vehicle
FC	Fuel Cell
PEMFC	Proton Exchange Membrane Fuel Cell
MEA	Membrane Electrode Assembly
CFD	Computational Fluid Dynamics
GDL	Gas Diffusion layer
SVM	Support Vector Machine
OCV	Open-Circuit Voltage

References

1. Ceschia, A.; Azib, T.; Bethoux, O.; Alves, F. Multi-Criteria Optimal Design for FUEL Cell Hybrid Power Sources. *Energies* **2022**, *15*, 3364. [CrossRef]
2. Wang, Y.; Zhang, Y.; Zhang, C.; Zhou, J.; Hu, D.; Yi, F.; Fan, Z.; Zeng, T. Genetic algorithm-based fuzzy optimization of energy management strategy for fuel cell vehicles considering driving cycles recognition. *Energy* **2023**, *263*, 126112. [CrossRef]
3. Nigmatullin, R.R.; Martemianov, S.; Evdokimov, Y.K.; Denisov, E.; Thomas, A.; Adiutantov, N. New approach for PEMFC diagnostics based on quantitative description of quasi-periodic oscillations. *Int. J. Hydrog. Energy* **2016**, *41*, 12582–12590. [CrossRef]
4. Available online: https://www.fch.europa.eu/page/call-2020/ (accessed on 2 June 2022).
5. Abdollahzadeh, M.; Ribeirinha, P.; Boaventura, M.; Mendes, A. Three-dimensional modeling of PEMFC with contaminated anode fuel. *Energy* **2018**, *152*, 939–959. [CrossRef]
6. Hwang, J.-J.; Dlamini, M.M.; Weng, F.-B.; Chang, T.; Lin, C.-H.; Weng, S.-C. Simulation of fine mesh implementation on the cathode for proton exchange membrane fuel cell (PEMFC). *Energy* **2022**, *244*, 122714. [CrossRef]
7. Rostami, L.; Haghshenasfard, M.; Sadeghi, M.; Zhiani, M. A 3D CFD model of novel flow channel designs based on the serpentine and the parallel design for performance enhancement of PEMFC. *Energy* **2022**, *258*, 124726. [CrossRef]
8. Carton, J.G.; Lawlor, V.; Olabi, A.G.; Hochenauer, C.; Zauner, G. Water droplet accumulation and motion in PEM (Proton Exchange Membrane) fuel cell mini-channels. *Energy* **2012**, *39*, 63–73. [CrossRef]
9. Zhong, Z.-D.; Zhu, X.-J.; Cao, G.-Y.; Shi, J.-H. A hybrid multi-variable experimental model for a PEMFC. *J. Power Sources* **2007**, *164*, 746–751. [CrossRef]
10. Legala, A.; Zhao, J.; Li, X. Machine learning modeling for proton exchange membrane fuel cell performance. *Energy AI* **2022**, *10*, 100183. [CrossRef]
11. Wang, Y.; Basu, S.; Wang, C.-Y. Modeling two-phase flow in PEM fuel cell channels. *J. Power Sources* **2008**, *179*, 603–617. [CrossRef]
12. Shen, J.; Xu, L.; Chang, H.; Tu, Z.; Chan, S.H. Partial flooding and its effect on the performance of a proton exchange membrane fuel cell. *Energy Convers. Manag.* **2020**, *207*, 112537. [CrossRef]
13. Bressel, M.; Hilairet, M.; Hissel, D.; Bouamama, B.O. Remaining Useful Life Prediction and Uncertainty Quantification of Proton Exchange Membrane Fuel Cell Under Variable Load. *IEEE Trans. Ind. Electron.* **2016**, *63*, 2569–2577. [CrossRef]
14. Jouin, M.; Gouriveau, R.; Hissel, D.; Péra, M.-C.; Zerhouni, N. Degradations analysis and aging modeling for health assessment and prognostics of PEMFC. *Reliab. Eng. Syst. Saf.* **2016**, *148*, 78–95. [CrossRef]

15. Pei, P.; Chang, Q.; Tang, T. A quick evaluating method for automotive fuel cell lifetime. *Int. J. Hydrog. Energy* **2008**, *33*, 3829–3836. [CrossRef]
16. Nguyen, H.L.; Han, J.; Vu, H.N.; Yu, S. Investigation of Multiple Degradation Mechanisms of a Proton Exchange Membrane Fuel Cell under Dynamic Operation. *Energies* **2022**, *15*, 9574. [CrossRef]
17. Benmouna, A.; Becherif, M.; Depernet, D.; Gustin, F.; Ramadan, H.S.; Fukuhara, S. Fault diagnosis methods for Proton Exchange Membrane Fuel Cell system. *Int. J. Hydrog. Energy* **2017**, *42*, 1534–1543. [CrossRef]
18. Talke, A.; Misz, U.; Konrad, G.; Heinzel, A. Influence of Nitrogen Compounds on PEMFC: A Comparative Study. *J. Electrochem. Soc.* **2018**, *165*, F3111–F3117. [CrossRef]
19. Chu, T.; Tang, Q.; Wang, Q.; Wang, Y.; Du, H.; Guo, Y.; Li, B.; Yang, D.; Ming, P.; Zhang, C. Experimental study on the effect of flow channel parameters on the durability of PEMFC stack and analysis of hydrogen crossover mechanism. *Energy* **2023**, *264*, 126286. [CrossRef]
20. Yousfi-Steiner, N.; Moçotéguy, P.; Candusso, D.; Hissel, D. A review on polymer electrolyte membrane fuel cell catalyst degradation and starvation issues: Causes, consequences and diagnostic for mitigation. *J. Power Sources* **2009**, *194*, 130–145. [CrossRef]
21. Yousfi Steiner, N.; Hissel, D.; Moçotéguy, P.; Candusso, D. Diagnosis of polymer electrolyte fuel cells failure modes (flooding and drying out) by neural networks modeling. *Int. J. Hydrog. Energy* **2011**, *36*, 3067–3075. [CrossRef]
22. Barbir, F.; Gorgun, H.; Wang, X. Relationship between pressure drop and cell resistance as a diagnostic tool for PEM fuel cells. *J. Power Sources* **2005**, *141*, 96–101. [CrossRef]
23. Li, H.; Tang, Y.; Wang, Z.; Shi, Z.; Wu, S.; Song, D.; Zhang, J.; Fatih, K.; Zhang, J.; Wang, H.; et al. A review of water flooding issues in the proton exchange membrane fuel cell. *J. Power Sources* **2008**, *178*, 103–117. [CrossRef]
24. Baumgartner, W.R.; Parz, P.; Fraser, S.D.; Wallnöfer, E.; Hacker, V. Polarization study of a PEMFC with four reference electrodes at hydrogen starvation conditions. *J. Power Sources* **2008**, *182*, 413–421. [CrossRef]
25. Xia, Z.; Chen, H.; Shan, W.; Zhang, R.; Zhang, T.; Pei, P. Behavior of current distribution evolution under reactant starvation conditions based on a single polymer electrolyte membrane fuel cell (PEMFC) with triple-serpentine flow field: An experimental study. *Int. J. Hydrog. Energy* **2023**, *S48*, 13650–13668. [CrossRef]
26. Taniguchi, A.; Akita, T.; Yasuda, K.; Miyazaki, Y. Analysis of degradation in PEMFC caused by cell reversal during air starvation. *Int. J. Hydrog. Energy* **2008**, *33*, 2323–2329. [CrossRef]
27. Manokaran, A.; Pushpavanam, S.; Sridhar, P. Dynamics of anode–cathode interaction in a polymer electrolyte fuel cell revealed by simultaneous current and potential distribution measurements under local reactant-starvation conditions. *J. Appl. Electrochem.* **2015**, *45*, 353–363. [CrossRef]
28. Narayanan, H.; Basu, S. Regeneration of CO poisoned Pt black anode catalyst in PEMFC using break-in procedure and $KMnO_4$ solution. *Int. J. Hydrog. Energy* **2017**, *42*, 23814–23820. [CrossRef]
29. Silva, R.E.; Harel, F.; Jemeï, S.; Gouriveau, R.; Hissel, D.; Boulon, L.; Agbossou, K. Proton Exchange Membrane Fuel Cell Operation and Degradation in Short-Circuit. *Fuel Cells* **2014**, *14*, 894–905. [CrossRef]
30. Tang, A.; Yang, L.; Zeng, T.; Yu, Q. Cascade Control Method of Sliding Mode and PID for PEMFC Air Supply System. *Energies* **2022**, *16*, 228. [CrossRef]
31. Bai, X.; Jian, Q.; Huang, B.; Luo, L.; Chen, Y. Hydrogen starvation mitigation strategies during the start-up of proton exchange membrane fuel cell stack. *J. Power Sources* **2022**, *520*, 230809. [CrossRef]
32. Chu, T.; Wang, Q.; Xie, M.; Wang, B.; Yang, D.; Li, B.; Ming, P.; Zhang, C. Investigation of the reversible performance degradation mechanism of the PEMFC stack during long-term durability test. *Energy* **2022**, *258*, 124747. [CrossRef]
33. Tang, H.; Qi, Z.; Ramani, M.; Elter, J.F. PEM fuel cell cathode carbon corrosion due to the formation of air/fuel boundary at the anode. *J. Power Sources* **2006**, *158*, 1306–1312. [CrossRef]
34. Chen, H.; Liu, Z.; Ye, X.; Yi, L.; Xu, S.; Zhang, T. Air flow and pressure optimization for air supply in proton exchange membrane fuel cell system. *Energy* **2022**, *238*, 121949. [CrossRef]
35. Durst, J.; Lamibrac, A.; Charlot, F.; Dillet, J.; Castanheira, L.F.; Maranzana, G.; Dubau, L.; Maillard, F.; Chatenet, M.; Lottin, O. Degradation heterogeneities induced by repetitive start/stop events in proton exchange membrane fuel cell: Inlet vs. outlet and channel vs. land. *Appl. Catal. Environ.* **2013**, *138–139*, 416–426. [CrossRef]
36. Bharath, K.V.S.; Blaabjerg, F.; Haque, A.; Khan, M.A. Model-Based Data Driven Approach for Fault Identification in Proton Exchange Membrane Fuel Cell. *Energies* **2020**, *13*, 3144. [CrossRef]
37. Zhang, L.; Bi, X.T.; Wilkinson, D.P.; Anderson, R.; Stumper, J.; Wang, H. Gas–liquid two-phase flow behavior in minichannels bounded with a permeable wall. *Chem. Eng. Sci.* **2011**, *66*, 3377–3385. [CrossRef]
38. Mortazavi, M.; Tajiri, K. Two-phase flow pressure drop in flow channels of proton exchange membrane fuel cells: Review of experimental approaches. *Renew. Sustain. Energy Rev.* **2015**, *45*, 296–317. [CrossRef]
39. Ijaodola, O.S.; El-Hassan, Z.; Ogungbemi, E.; Khatib, F.N.; Wilberforce, T.; Thompson, J.; Olabi, A.G. Energy efficiency improvements by investigating the water flooding management on proton exchange membrane fuel cell (PEMFC). *Energy* **2019**, *179*, 246–267. [CrossRef]
40. Hussaini, I.S.; Wang, C.-Y. Visualization and quantification of cathode channel flooding in PEM fuel cells. *J. Power Sources* **2009**, *187*, 444–451. [CrossRef]

41. Grimm, M.; See, E.J.; Kandlikar, S.G. Modeling gas flow in PEMFC channels: Part I—Flow pattern transitions and pressure drop in a simulated ex situ channel with uniform water injection through the GDL. *Int. J. Hydrog. Energy* **2012**, *37*, 12489–12503. [CrossRef]
42. Yousfi-Steiner, N.; Moçotéguy, P.; Candusso, D.; Hissel, D.; Hernandez, A.; Aslanides, A. A review on PEM voltage degradation associated with water management: Impacts, influent factors and characterization. *J. Power Sources* **2008**, *183*, 260–274. [CrossRef]
43. Springer, T.E.; Zawodzinski, T.A.; Gottesfeld, S. Polymer Electrolyte Fuel Cell Model. *J. Electrochem. Soc.* **1991**, *138*, 2334–2342. [CrossRef]
44. Dicks, A.; Rand, D.A.J. *Fuel Cell Systems Explained*, 3rd ed.; Wiley: Hoboken, NJ, USA, 2018.
45. Belhaj, F.Z.; El Fadil, H.; El Idrissi, Z.; Intidam, A.; Koundi, M.; Giri, F. New Equivalent Electrical Model of a Fuel Cell and Comparative Study of Several Existing Models with Experimental Data from the PEMFC Nexa 1200 W. *Micromachines* **2021**, *12*, 1047. [CrossRef] [PubMed]
46. Talj, R.; Azib, T.; Béthoux, O.; Remy, G.; Marchand, C.; Berthelot, E. Parameter analysis of PEM fuel cell hysteresis effects for transient load use. *Eur. Phys. J. Appl. Phys.* **2011**, *54*, 23410. [CrossRef]
47. Dhirde, A.M.; Dale, N.V.; Salehfar, H.; Mann, M.D.; Han, T.-H. Equivalent Electric Circuit Modeling and Performance Analysis of a PEM Fuel Cell Stack Using Impedance Spectroscopy. *IEEE Trans. Energy Convers.* **2010**, *25*, 778–786. [CrossRef]
48. Zuo, J.; Lv, H.; Zhou, D.; Xue, Q.; Jin, L.; Zhou, W.; Yang, D.; Zhang, C. Long-term dynamic durability test datasets for single proton exchange membrane fuel cell. *Data Brief* **2021**, *35*, 106775. [CrossRef]
49. Ceschia, A. Méthodologie de Conception Optimale de Chaines de Conversion d'énergie Embarquées 186. Ph.D. Thesis, Université Paris-Saclay, Paris, France, 2020.
50. Dataset: IEEE PHM Data Challenge 2014. Available online: http://dx.doi.org/doi:10.25666/DATAUBFC-2021-07-19 (accessed on 2 June 2022).
51. Karnik, A.Y.; Stefanopoulou, A.G.; Sun, J. Water equilibria and management using a two-volume model of a polymer electrolyte fuel cell. *J. Power Sources* **2007**, *164*, 590–605. [CrossRef]
52. Lockhart, R.W. Proposed Correlation of Data for Isothermal Two-Phase, Two-Component Flow in Pipes. *Chem. Eng. Prog.* **1949**, *45*, 39–48.
53. Available online: https://www.heliocentrisacademia.com/asset/160/Datasheet_Nexa1200_EN.pdf/ (accessed on 2 June 2022).